

Exposing the dead cone effect with jet substructure techniquesFabio Maltoni,^{1,*} Michele Selvaggi,^{1,†} and Jesse Thaler^{2,‡}¹*Centre for Cosmology, Particle Physics and Phenomenology CP3, Université Catholique de Louvain, Chemin du Cyclotron, 1348 Louvain la Neuve, Belgium*²*Center for Theoretical Physics, Massachusetts Institute of Technology, Cambridge, Massachusetts 02139, USA*

(Received 27 June 2016; published 14 September 2016)

The dead cone is a well-known effect in gauge theories, where radiation from a charged particle of mass m and energy E is suppressed within an angular size of m/E . This effect is universal as it does not depend on the spin of the particle nor on the nature of the gauge interaction. It is challenging to directly measure the dead cone at colliders, however, since the region of suppressed radiation either is too small to be resolved or is filled by the decay products of the massive particle. In this paper, we propose to use jet substructure techniques to expose the dead cone effect in the strong-force radiation pattern around boosted top quarks at the Large Hadron Collider. Our study shows that with 300/fb of 13–14 TeV collision data, ATLAS and CMS could obtain the first direct evidence of the dead cone effect and test its basic features.

DOI: 10.1103/PhysRevD.94.054015

I. INTRODUCTION

When charged particles are produced in high-energy collisions, they are usually accompanied by final-state radiation (FSR). This process is familiar in quantum electrodynamics, where electrons radiate photons, as well as in quantum chromodynamics (QCD), where quarks (and gluons) radiate gluons. The pattern of radiation depends crucially on the mass of the emitter but not on its spin, leading to the famous *dead cone* effect [1–3] where radiation from quarks with mass m_q and energy E_q is suppressed for emission angles $\theta \lesssim m_q/E_q$. The dead cone is a fundamental prediction of QCD and other gauge theories, relying on only the behavior of radiation from massive particles in the soft (and collinear) limit.

While the prediction of the dead cone effect is uncontroversial, actually measuring the dead cone radiation pattern in QCD has turned out to be extremely challenging. The reason is simple: massive particles decay, and the same angular scale m/E appears both in the dead cone effect as well as in the characteristic opening angle between the decay products. In this way, the dead cone is effectively “filled,” so, while the overall suppression of gluon radiation for heavy quarks can be inferred through inclusive [4–8] or semi-inclusive [9–11] observables, the universal angular radiation pattern around the massive particle is obscured. More direct probes of the dead cone for bottom and charm quarks have been put forward, for example in e^+e^- collisions at LEP [12,13] and in ep collisions at HERA [14], and the dead cone effect is included in the shower deconstruction approach to top tagging [15]. To our

knowledge, though, no definitive dead cone measurement has been made to date.

In this paper, we propose to directly measure the dead cone around top quarks at the Large Hadron Collider (LHC) using jet substructure techniques [16–19]. This direct approach is interesting both as a fundamental test of gauge theories and as a way to validate the treatment of radiation from massive particles in Monte Carlo generators. Our focus is on leptonic decays, where a high-energy top quark can emit FSR gluons before decaying to a charged lepton, neutrino, and bottom quark. Because $m_b/E_b \ll 1$ in top decays, the dead cone effect for the bottom quark is negligible, yet bottom-quark FSR is abundant and it tends to fill the top-quark dead cone region. Using recursive jet clustering algorithms, though, we show how to statistically separate radiation from the top and bottom, thereby revealing the top-quark dead cone pattern.

Our method relies on soft drop declustering [20] (see also Refs. [21–25]), a jet substructure technique that removes soft radiation from a jet to identify the hard jet core. In Ref. [26], soft drop was applied to light quark and gluon jets to expose the famous Altarelli-Parisi splitting functions [27] which encode the energy pattern of FSR. Here, we apply a similar technique to boosted top-quark jets, focusing now on the angular pattern of FSR. While simple in its essence, our method relies on several key steps, such as the reconstruction of the top momentum despite the lost neutrino, whose robustness we test using parton shower (PS) generators.

The rest of this paper is organized as follows. In Sec. II, we review the dead cone effect in the idealized context of stable top quarks in electron-positron collisions. In Sec. III, we discuss subtleties related to top decay and the contamination coming from initial state radiation (ISR) and underlying event (UE). We present our novel measurement

*fabio.maltoni@uclouvain.be

†michele.selvaggi@uclouvain.be

‡jthaler@mit.edu

strategy in Sec. IV and estimate the LHC sensitivity with 300 fb^{-1} in Sec. V. We discuss subdominant backgrounds in Sec. VI and conclude in Sec. VII, leaving additional cross-checks to the Appendixes.

II. IDEALIZED TOP DEAD CONE

We begin with the idealized case of top pair production in electron-positron collisions, $e^+e^- \rightarrow t\bar{t}$, where we treat the top quark as stable. This approximation allows us to study the pattern of QCD radiation from the top quarks at various levels of accuracy without having to consider the top-quark decay products.

At tree level, each top quark carries three-momentum $p_t = \sqrt{E_t^2 - m_t^2}$ and energy $E_t = \sqrt{s}/2$, where \sqrt{s} is the e^+e^- collision energy.¹ In the soft and collinear limit, the probability for a top quark to emit a FSR gluon with energy fraction z and opening angle θ is [1–3]

$$\frac{1}{\sigma} \frac{d^2\sigma}{dzd\theta^2} \simeq \frac{\alpha_s}{\pi} C_F \frac{1}{z} \frac{\theta^2}{(\theta^2 + \theta_D^2)^2}, \quad (1)$$

where α_s is the strong coupling constant, $C_F = 4/3$ is the top-quark color factor, $m_t \simeq 173 \text{ GeV}$ is the top mass, and

$$\theta_D \equiv \frac{m_t}{p_t} \simeq \frac{m_t}{E_t} \quad (2)$$

is the dead cone angle. The relation $\theta_D \simeq m_t/E_t$ is valid already for moderately relativistic tops (e.g. $p_t \gtrsim 2m_t$), so we use this approximation throughout. The emission probability in Eq. (1) reaches its maximum at $\theta \simeq \theta_D$ and is suppressed for angles $\theta \lesssim \theta_D$ (i.e. a dead cone). In the large Lorentz boost limit $m_t/E_t \ll 1$, one recovers the usual collinear divergence for gluon emissions from massless quarks. It is a remarkable property of the soft limit that the angular dependence in Eq. (1) is universal and does not depend on the spin of the massive particle.

To visualize the dead cone, in Fig. 1 we show the full matrix element (ME) at next-to-leading order (NLO) from MADGRAPH5_AMC@NLO 2.3.2 (MG5aMC) [28], i.e. $\mathcal{O}(\alpha_s^2)$ with up to two additional final-state partons (typically two gluons). Here, we have defined

$$\Theta \equiv \frac{\theta}{\theta_D}, \quad X \equiv \Theta \cos \phi, \quad Y \equiv \Theta \sin \phi, \quad (3)$$

such that the top flight direction is at $(X, Y) = (0, 0)$ and the dead cone peak is at $\Theta^2 = X^2 + Y^2 \simeq 1$. The effective $t^* \rightarrow tg$ kinematics are determined by forcing the top quark to be stable and taking the “gluon” to be the vector sum of all radiated particles that are closer to the top than to the

¹Throughout this paper, the “ t ” subscript indicates the top quark, not to be confused with p_T indicating transverse momentum with respect to the beam line in LHC collisions.

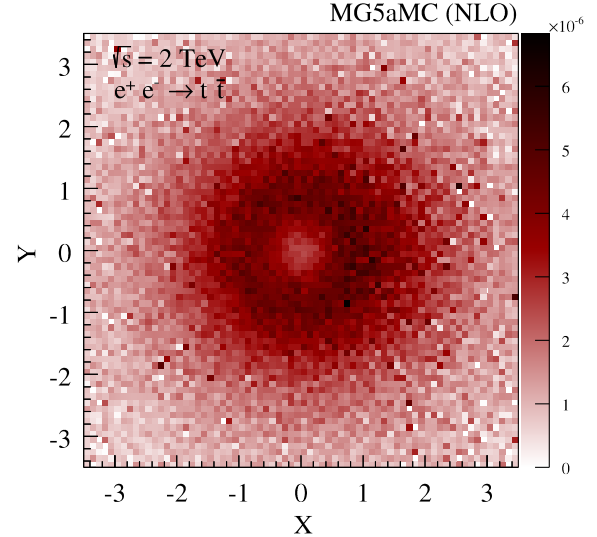


FIG. 1. Idealized gluon radiation pattern for $e^+e^- \rightarrow t\bar{t}$ at $\sqrt{s} = 2 \text{ TeV}$, showing the expected dead cone suppression at the origin. This is a NLO calculation with up to two additional partons in the final state. To define the effective $t^* \rightarrow tg$ kinematics, the gluon corresponds to the sum of emissions within the top hemisphere, imposing a cut of $E_g > 50 \text{ GeV}$. The X and Y coordinates are then normalized such that the dead cone peak is at $X^2 + Y^2 \simeq 1$.

antitop, effectively partitioning the event into top and antitop hemispheres.² This distribution is for $\sqrt{s} = 2 \text{ TeV}$ after imposing a cut on the gluon of $E_g > 50 \text{ GeV}$.

In Fig. 2, we plot the idealized analytic distribution in Eq. (1) together with the corresponding distributions obtained from the exact LO and NLO fixed-order calculations for $e^+e^- \rightarrow t\bar{t}j$. This comparison shows that the dead cone radiation pattern is stable under radiative corrections and agrees well with the analytic approximation in Eq. (1). The deviations at LO near $\Theta^2 \simeq 0$ can be largely attributed to the $E_g > 50 \text{ GeV}$ cut, which forces us away from the strict soft limit [as motivated by the discussion around Eq. (7) below]. Though not shown here, we tested that the expected $1/z$ behavior in Eq. (1) is also seen in the fixed-order calculations.

As a next step towards a realistic modeling of the radiation from a top quark, we consider the impact of multiple gluon emissions using PS generators. In PYTHIA 8.219 [29,30], the dead cone effect is implemented via ME corrections [31]. These ME corrections can also be turned off, an option we exploit later to define a null test.³ In Fig. 3(a), we compare the PYTHIA distributions for Θ^2

²Different definitions of the gluon will change the precise shape of the dead cone. We use jet substructure techniques in Sec. IV, starting from a jet cone of radius $R = 1.0$.

³We thank Torbjörn Sjöstrand for resolving a bug in PYTHIA 8.215 that obscured the dead cone effect. The proper ME corrections are applied from PYTHIA 8.219 on.

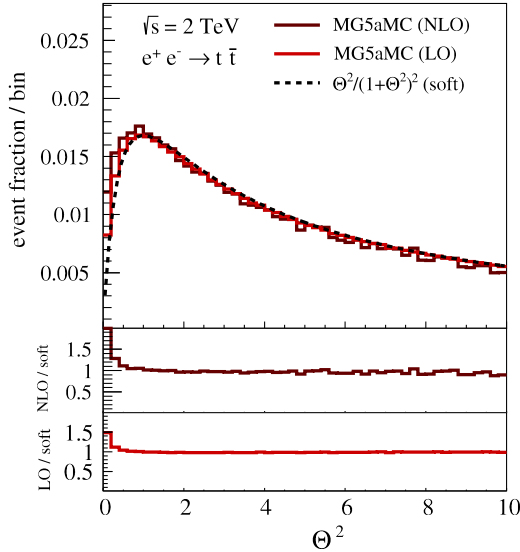


FIG. 2. Idealized distributions for $\Theta^2 = X^2 + Y^2$ in $e^+e^- \rightarrow t\bar{t}$ at $\sqrt{s} = 2$ TeV, comparing LO and NLO calculations to the universal form in Eq. (1).

with and without the dead cone effect. One can clearly see the collinear peak at $\Theta^2 = 0$ when the corrections are off and the expected dead cone suppression for $\Theta^2 \lesssim 1$ when the corrections are on. In this plot, the distributions have a common normalization such that the ME-corrected distribution integrates to unity.

In Fig. 3(b), we compare PYTHIA 8.219 [29,30] to HERWIG 2.7.1 [32] and SHERPA 2.2.0 [33] as well as to fixed-order LO and NLO distributions from MADGRAPH5_AMC@NLO 2.3.2 [28]. In this case, we normalize the distributions to unity to emphasize any possible shape differences. The predictions from PS generators feature the dead cone suppression for $\Theta^2 < 1$, in quite good agreement (better than 10%) with NLO fixed-order predictions, clearly displaying the expected universal behavior.

III. TOP DECAY AND CONTAMINATING RADIATION

We now pass from the idealized case above where the top quark has been treated as stable to the realistic case involving effects due to its decay. The top quark has a very short lifetime and decays almost exclusively to a bottom quark and a weak boson ($t \rightarrow bW$). The W boson has a large ($\approx 68\%$) branching fraction to hadronic final states, yet, in order to avoid unnecessary further contamination of the dead cone, we focus on leptonic decays ($W \rightarrow \ell\nu$). Because the b quark is a colored particle, its contamination of the top dead cone due to radiation and fragmentation is unavoidable and needs to be carefully examined.

At leading order, two different gluon emission processes can be identified, as shown in Fig. 4. The signal process

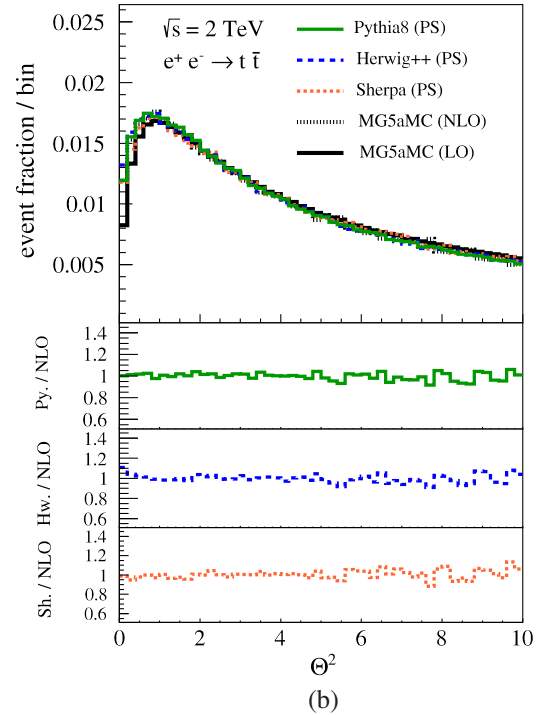
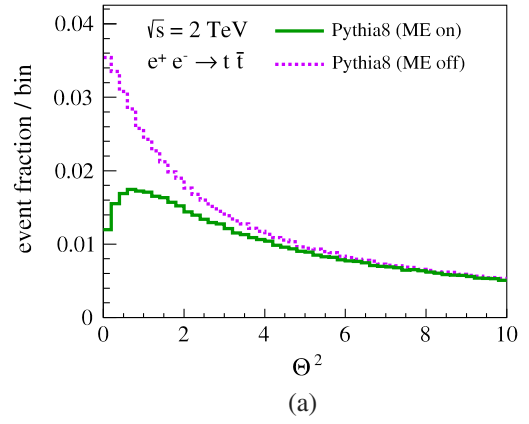


FIG. 3. The same as Fig. 2, but now considering PS predictions. (a) Turning ME corrections off and on in PYTHIA. With ME corrections off, an erroneous collinear peak is seen at $\Theta^2 = 0$. With ME corrections on, the dead cone is apparent for $\Theta^2 \lesssim 1$. (b) Comparing PYTHIA, HERWIG, and SHERPA PS generators to LO and NLO fixed-order calculations.

which features the dead cone is FSR top-quark radiation, corresponding to an off-shell top emitting a gluon and going on shell [see Fig. 4(a)]:

$$S: t^* \rightarrow tg. \quad (4)$$

This is the process that defines the dead cone distribution in Eq. (1). The background process where the dead cone is absent is gluon emission during on-shell top decay [see Fig. 4(b)]:

$$B_{1,2}: t \rightarrow bWg. \quad (5)$$

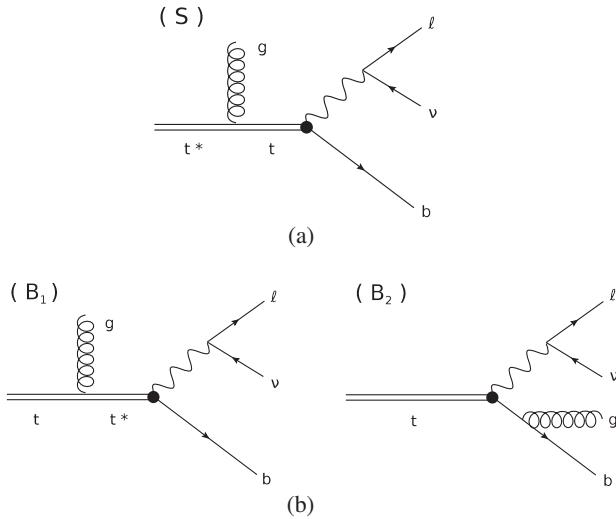


FIG. 4. Feynman diagrams for gluon radiation in (a) the signal process of top FSR $t^* \rightarrow tg$ and (b) the background process of top decay $t \rightarrow bWg$.

Even though diagrams S and B_1 both have an off-shell top propagator, B_1 does not contribute to the dead cone effect. This is easiest to see in limit that the top quark is exactly stable. Specifically, one can boost to the on-shell top rest frame, where it is then apparent that the emitted gluon in diagram B_1 is uncorrelated with the initial top momentum direction. Because the top is unstable, though, there is interference between the signal and background processes proportional to the top-quark width $\Gamma_t \approx 1.4$ GeV. This interference becomes relevant when

$$2p_t \cdot p_g \sim m_t \Gamma_t, \quad (6)$$

where p_t and p_g are the top and gluon 4-momenta. Indeed, observables have been proposed to exploit this interference regime and potentially measure the top-quark width [34–36].

Here, our goal is to isolate the S process, so we want to avoid interference effects. In addition, if the gluon energy is too small, then there is no practical way to distinguish an on-shell top from an off-shell top, allowing the $B_{1,2}$ diagrams to “bleed through” into the S diagram signal region. To estimate when interference effects can be neglected, we use the relation $2p_t \cdot p_g \sim E_t E_g \theta_D^2$ for sufficiently small angles in the lab frame, leading to the requirement

$$z \equiv \frac{E_g}{E_t} \gg \frac{\Gamma_t}{m_t}, \quad (7)$$

which for $\Gamma_t/m_t \approx 0.01$ implies $z \gtrsim \mathcal{O}(0.1)$. In Appendix A, we explicitly check that Eq. (7) with $z > 0.05$ is sufficient to suppress the combined interference and bleed-through effects. We consider further kinematic selections to suppress the decay processes in the next section.

We conclude this section by commenting on additional sources of background that are present in pp collisions coming from ISR and UE. Radiation associated with the initial partons involved in the scattering as well as with soft QCD effects from the proton remnants can “accidentally” end up in the vicinity of the reconstructed top quark. Because top quarks are dominantly produced via gluon fusion at the LHC, and because the degree of ISR is controlled by the gluon color factor $C_A = 3$, ISR turns out to be a rather important source of dead cone contamination. In addition, UE contributes to an overall pedestal in the Θ^2 distribution which also fills in the dead cone region. This motivates the use of jet grooming techniques to mitigate the impact of ISR or UE contamination.

IV. EXPOSING THE DEAD CONE AT THE LHC

We now present an analysis strategy to observe the dead cone effect at the LHC. Our starting point is an event sample of boosted top-quark pairs, with one top quark decaying hadronically and the other one leptonically. The boosted leptonic top (BLT) is where we propose to measure the dead cone effect.

The reason for considering large Lorentz boosts is that top FSR is roughly proportional to $\alpha_s \log(E_t/m_t)$. By going to larger values of E_t , the overall level of FSR is enhanced, making the dead cone suppression more distinct. We consider top quarks with transverse momenta of $p_T \gtrsim 500$ GeV for which the expected dead cone angle is $\theta_D \approx 0.3$, safely larger than the angular resolution of the LHC detectors.

The reason for considering single-lepton top pairs is threefold. First, identifying a boosted hadronic top ensures high signal purity when using jet substructure tagging techniques [37]. Second, the single-lepton selection ensures that the primary source of missing energy comes from the single neutrino in the event, allowing an accurate reconstruction of the BLT direction. Third, performing the measurement on the BLT avoids hadronic dead cone contamination from the decaying W boson. As discussed in Sec. III, residual contamination of the top dead cone comes mainly from b -quark FSR as well as from ISR and UE.

A. Event selection

Our baseline event selection involved two large radius ($R = 1.0$) “fat” jets at central rapidities ($|\eta^j| < 2.5$) and high transverse momenta ($p_T^j > 300$ GeV). Jets are reconstructed using the anti- k_T jet algorithm [38] from FASTJET 3.1.3 [39]. Exactly one of the two fat jets is required to satisfy a boosted hadronic top tag ($p_T^j > 500$ GeV), and we use Ref. [37] to estimate the tagging performance. The other jet is promoted to a BLT candidate if it contains at least one high- p_T lepton ($p_T^l > 50$ GeV). To avoid misreconstructing the BLT kinematics due to collinear photon

FSR, we define the effective lepton four-vector to include all photons within $\Delta R_{\gamma\ell} < 0.1$. We further require large missing transverse momentum ($p_T^{\text{miss}} > 50$ GeV).

The above selection is designed to obtain high purity of BLT signal events. To further increase the signal yield, one could lower the top p_T threshold and possibly widen the jet radius, though we found that this did not improve the statistical significance of the dead cone effect. Additional potential backgrounds are discussed in Sec. VI, though they are expected to only appear at the few-percent level.

B. Object reconstruction

From the BLT constituents, we next need to define the b quark, FSR gluon (g), lepton (ℓ), and neutrino (ν) candidates. In addition, we want to mitigate the impact of contamination from ISR or UE, as well as from pileup at higher luminosities.

To identify the b and g candidates and suppress contamination, we exploit recent advances in jet substructure. After removing the high p_T lepton (and its collinear photon FSR), the BLT constituents are reclustered with the Cambridge-Aachen (C/A) algorithm [40], which reorganizes the BLT constituents into an angular-ordered tree. We then apply the soft drop algorithm [20], which aims to remove soft contamination from the fat jet and isolate two subjets within the BLT. Soft drop works by recursively declustering the C/A tree, removing the softer branch until

$$\frac{\min[p_{T1}, p_{T2}]}{p_{T1} + p_{T2}} > z_{\text{cut}} \left(\frac{R_{12}}{R} \right)^\beta, \quad (8)$$

where p_{Ti} are the transverse momenta of the subjets, R_{12} is their rapidity-azimuth distance, and R is the initial jet radius. For this study, we use the parameters

$$\beta = 0, \quad z_{\text{cut}} = 0.05. \quad (9)$$

By choosing $\beta = 0$, soft drop behaves similarly to the modified mass drop tagger with $\mu = 1$ [25]. In order to increase the signal acceptance, we have selected the z_{cut} value to be a bit looser than the 0.1 value used in Refs. [20,26,41].

If soft drop finds no substructure within the hadronic component of the BLT jet, the event is discarded. If soft drop instead finds evidence for a two-prong substructure, then the 4-momenta of two subjet components are returned. Out of the two subjets found by soft drop, exactly one subjet is required satisfy a b tag to become our b quark candidate. The remaining subjet is our gluon candidate, which ideally would come from the top FSR signal. We further impose $p_T^b > 50$ GeV and $p_T^g > 25$ GeV to avoid pathological configurations.

To identify the neutrino candidate, we use the W mass constraint on the $\ell\nu$ system to solve for the missing

neutrino longitudinal momentum component. Strictly speaking, the W mass constraint yields two solutions for the neutrino longitudinal momentum, so we choose the one that gives the smallest value of $\min\{|m_t - m_{b\ell\nu}|, |m_t - m_{b\ell\nu g}|\}$. By considering both the $b\ell\nu$ and $b\ell\nu g$ systems, we avoid sculpting an artificial dead cone region. After reconstructing the neutrino direction, we now have a BLT candidate with well-defined b , ℓ , ν , and g constituents.

Finally, we impose a cut on the gluon momentum relative to the reconstructed BLT momentum in order to satisfy the interference and bleed-through requirement from Eq. (7):

$$\frac{p_T^g}{p_T^t} > 0.05. \quad (10)$$

Note that this requirement is stricter than the z_{cut} requirement of the soft drop algorithm, which only constrains the gluon momentum relative to the momentum of the top minus W system. In practice, Eq. (10) is often satisfied already by the $p_T^g > 25$ GeV requirement, since the typical top p_T for this selection is 500 GeV.

C. Signal isolation

With the BLT kinematics in hand, we now take advantage of the differing kinematics in top FSR and top decay. When the gluon is radiated in top FSR then $m_{b\ell\nu} \approx m_t$ and $m_{b\ell\nu g} > m_t$, whereas when the gluon is radiated in top decay then $m_{b\ell\nu} < m_t$ and $m_{b\ell\nu g} \approx m_t$. These two regions can be seen clearly in Fig. 5, from a LO calculation where all of the above selection criteria are applied.⁴

We therefore have a signal-enriched phase space region where the dead cone effect should be enhanced and a background-enriched control region where no dead cone is expected:

$$S\text{-enriched: } m_{b\ell\nu} \in [170, 200] \text{ GeV}, \quad (11)$$

$$B\text{-enriched: } m_{b\ell\nu} < 160 \text{ GeV}. \quad (12)$$

While one might try to cut on $m_{b\ell\nu g}$ to further enhance top FSR and suppress top decay in the S -enriched region, we find that this sculpts an artificial dead cone since it preferentially selects events with wide-angle gluons.

At this point, it is convenient to rotate the event such that the momentum of the reconstructed BLT (including the radiated gluon) points in the z direction, and the b -subjet

⁴For reasons of computational efficiency, this LO calculation is for $pp \rightarrow t_{\text{had}} b\ell\nu g$, where t_{had} refers to a hadronic top quark that is treated as stable. While strictly speaking not gauge invariant when the leptonic top is off shell, this amplitudes provides an excellent approximation to the full one, with a negligible uncertainty in our analysis.

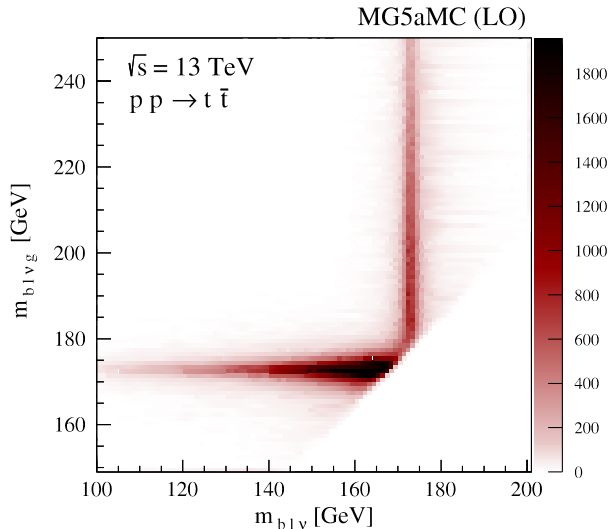


FIG. 5. Invariant mass of $b\ell\nu$ versus $b\ell\nu g$ after the soft drop procedure, showing the regions that are signal enriched (vertical bar) and background enriched (horizontal bar) at LO.

candidate has a vanishing y component and negative x component. This allows us to isolate (and better visualize) backgroundlike configurations where the gluon candidate is likely to come from b -quark FSR ($x < 0$, dominated by diagram B_2) from signal-like configurations where the gluon candidate is likely to come from top-quark FSR ($x > 0$, diagram S). As in Eq. (3), we rescale the gluon kinematics to X and Y coordinates; this ensures that the expected dead cone boundary is at $\Theta^2 = 1$ regardless of the reconstructed top momentum.⁵

The resulting gluon radiation pattern is shown in Fig. 6. In both the S - and B -enriched samples, there is a prominent peak near $(X, Y) = (-1, 0)$, corresponding roughly to the b quark location. This peak is expected, since even with the S -enriched selection, there is still residual contamination from b -quark FSR. For the S -enriched sample there is a faint disk of radiation within $\Theta^2 \lesssim 1$, though scant evidence for dead cone depletion near the $\Theta = 0$ origin. This disk corresponds to the desired top FSR signal seen in the idealized distribution from Fig. 1. No such disklike feature is observed in the B -enriched sample, giving us confidence that the S -enriched selection has properly isolated the top FSR of interest.

In Appendix B, we show distributions for the observable

$$\Theta_S^2 \equiv \text{sgn}(X)\Theta^2, \quad (13)$$

⁵To better match the discussion in Sec. II, we define the Θ coordinate in terms of lab-frame energies and angles, instead of the more familiar p_T and ΔR . The difference is negligible for narrow jets and only leads to a small distortion for the $R = 1.0$ jet radius used here.

such that $\Theta_S^2 > 0$ isolates the phase space region away from the b quark direction. However, with no further cuts, the realistic dead cone structure in Fig. 6(a) is rather muted compared to the idealized dead cone structure in Fig. 1. One might therefore wonder if there are additional kinematic handles to enhance the dead cone effect and observe a suppression near $\Theta = 0$.

D. Further optimization

The most obvious source of dead cone contamination is b -quark FSR. By two-body kinematics, the typical opening angle between the b quark direction and the initial top-quark direction is typically *the same* as the dead cone angle, $\theta_{tb} \approx \theta_D$. Moreover, the total gluon FSR from the b quark is expected to be larger than from the top quark.⁶ While imposing a $\Theta_S^2 > 0$ restriction could help isolate the phase space region away from the b quark, a more aggressive way to “clean up” the dead cone region is to force the b candidate to have a large value of Θ_b .

In Fig. 7, we show the impact of a $\Theta_b > 1.0$ restriction. Such a cut (which could be optimized in a full analysis) ensures that b -quark FSR is typically away from the dead cone region $\Theta^2 \lesssim 1$. Because this does not impose any criteria on the gluon subjet, this selection does not sculpt a dead cone, though it does preferentially select top decays where the b quark flies perpendicular to the top boost direction in the top rest frame.

With this $\Theta_b > 1.0$ cut in place, we project down to the Θ_S^2 observable from Eq. (13) in Fig. 8. Focusing on $\Theta_S^2 > 0$ for the S -enriched sample in Fig. 8(a), the dead cone structure is quite visible. When turning the ME corrections off in PYTHIA, one sees a rise towards $\Theta_S^2 = 0$, corresponding to FSR emitted collinear to the initial top direction. With the ME corrections on, the dead cone region at $\Theta_S^2 \lesssim 1$ appears as expected. No such features are seen in the B -enriched sample in Fig. 8(b), suggesting that Θ_S^2 is a useful test for the dead cone effect at the LHC, especially after a cut on Θ_b . Comparing different predictions in Fig. 8(c), we see that each generator predicts some degree of dead cone suppression for $\Theta_S^2 \lesssim 1$, though the precise size and shape differs noticeably, motivating future higher-order calculations of the dead cone effect in pp collisions. Even without new calculations, these generator differences indicate that a direct measurement of the dead cone effect at the LHC would help test Monte Carlo treatments of gluon radiation from massive quarks.

⁶Bottom FSR is proportional to $\alpha_s \log(E_b^*/m_b)$, where E_b^* is the bottom energy in the top rest frame, while top FSR is proportional to $\alpha_s \log(E_t^*/m_t)$, where E_t^* is the top energy in the $t\bar{t}$ rest frame, so the former dominates at the moderate top boosts considered here.

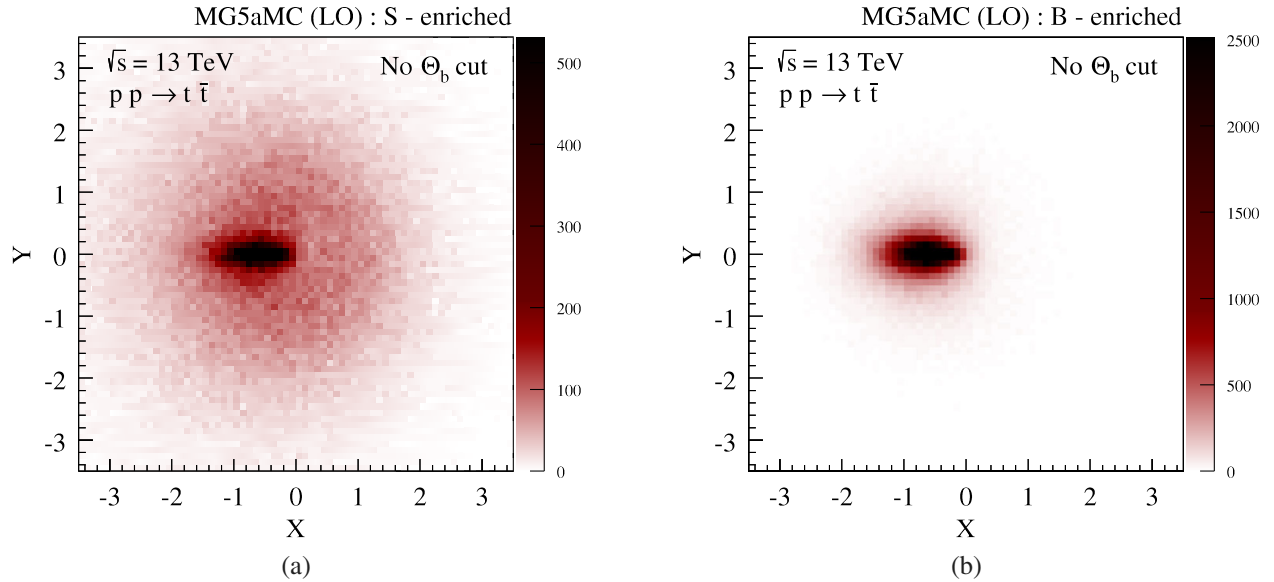


FIG. 6. Realistic angular distribution for gluon radiation in 13 TeV LHC collisions at LO. The event is rotated such that the reconstructed top flight direction is at $(X, Y) = (0, 0)$ and the b jet points along the negative X axis. (a) The S -enriched region ($m_{b\ell\nu} \in [170, 200]$ GeV), showing a disk of top FSR within $\Theta^2 \lesssim 1$ along with contamination from b quark FSR at $X < 0$. (b) The B -enriched region ($m_{b\ell\nu} < 160$ GeV) where no disklike top FSR pattern is expected (or observed). See Fig. 7 for further cuts to isolate the top dead cone suppression at $\Theta = 0$.

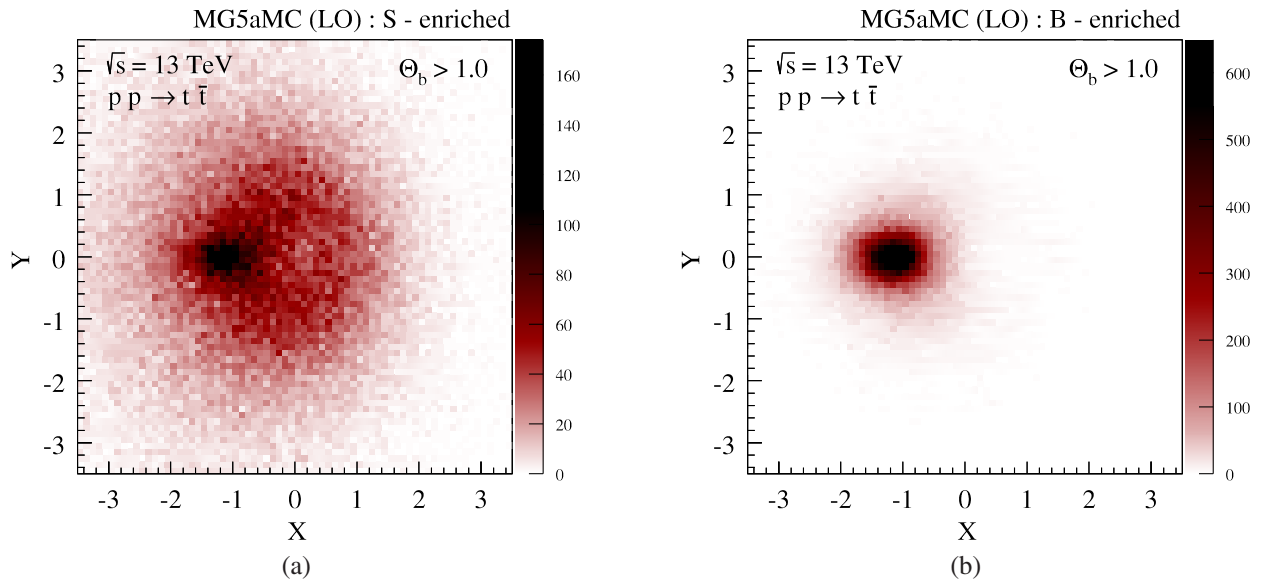


FIG. 7. The same as Figs. 6(a) and 6(b), but applying a cut on the b quark candidate of $\Theta_b > 1.0$. The dead cone effect at $\Theta = 0$ is noticeably enhanced in the S -enriched region without sculpting a feature in the B -enriched region.

One particular challenge in pp collisions that is absent from e^+e^- collisions is ISR and UE. This background has no preferred orientation with respect to the top flight direction and simply leads to uniform contamination of the dead cone region, which is only partially mitigated by soft drop. In Appendix C, we show $e^+e^- \rightarrow t\bar{t}$ collisions

with the identical event selection as used in the pp case, where the dead cone effect is more readily visible. Though not shown here, we also tested our analysis strategy on just the $q\bar{q} \rightarrow t\bar{t}$ subprocess where ISR contamination is somewhat suppressed, yielding results that are intermediate between the e^+e^- and full pp distributions.

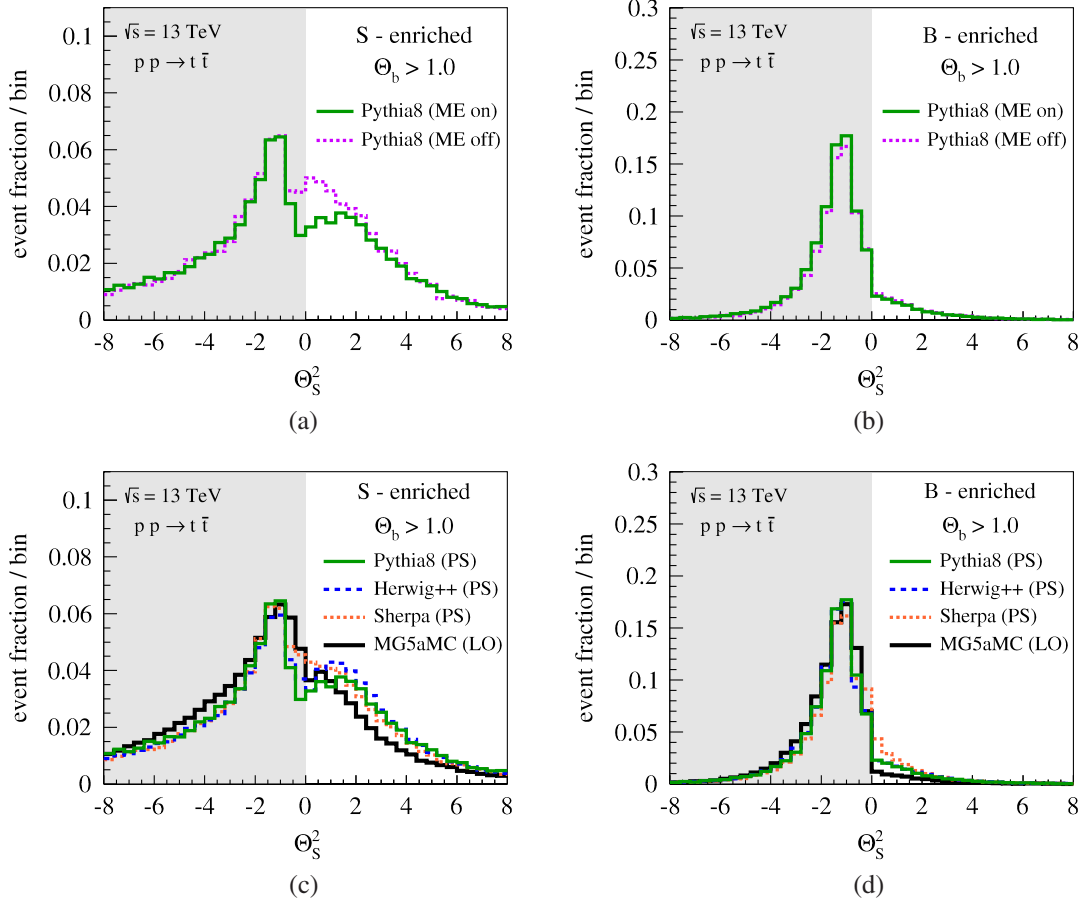


FIG. 8. Realistic distributions for $\Theta_S^2 = \text{sgn}(X)(X^2 + Y^2)$ in 13 TeV LHC collisions, for the (left column) S -enriched and (right column) B -enriched samples. Here, a cut of $\Theta_b > 1.0$ has been applied; see Fig. 10 for distributions without this cut. (Top row) Turning ME corrections off and on in PYTHIA. Restricting one's attention to $\Theta_S^2 \in [0, 1]$ for the S -enriched sample, one sees qualitatively the same dead cone physics as in Fig. 3(a). ME corrections have a negligible impact for the B -enriched sample. (Bottom row) Comparing the PS generators to LO fixed-order calculations. While each generator shows some evidence for a dead cone suppression, the quantitative behavior is noticeably different.

V. ESTIMATED LHC SENSITIVITY

Because the top dead cone in Fig. 8(a) is still rather subtle, large data samples will be necessary to find conclusive evidence for this effect. For an integrated luminosity \mathcal{L} and signal efficiency ϵ_{total} , the expected number of events \mathcal{N} contributing to the S -enriched sample can be expressed as

$$\mathcal{N} = \mathcal{L} K \sigma^{\text{LO}}(pp \rightarrow t\bar{t}, p_T^{t,\bar{t}} > 500 \text{ GeV}) \times \mathcal{B}(t\bar{t} \rightarrow t_{\text{had}} t_{\text{lep}}) \epsilon_{\text{total}}. \quad (14)$$

Here, $\sigma(pp \rightarrow t\bar{t}, p_T^{t,\bar{t}} > 500 \text{ GeV}) = 1.4 \text{ pb}$ is the boosted top cross section at LO, $K = 1.65$ is the ratio of the inclusive 13 TeV $pp \rightarrow t\bar{t}$ cross sections at NNLO [42] compared to LO, and $\mathcal{B}(t\bar{t} \rightarrow t_{\text{had}} t_{\text{lep}}) = 0.30$ is the fraction of top-quark pairs featuring a single-lepton final state.

The total signal efficiency can be expressed as

$$\epsilon_{\text{total}} \equiv \epsilon_{\text{fid}} \epsilon_{\text{top}} \epsilon_{\text{SD}} \epsilon_b \epsilon_{\Theta_b} \epsilon_S. \quad (15)$$

Using PYTHIA, we estimate the efficiency of the fiducial cuts ($p_T^j > 300 \text{ GeV}$, $p_T^l > 500 \text{ GeV}$, $|\eta^{j,l}| < 2.5$, $p_T^{\text{miss}} > 50 \text{ GeV}$, and $p_T^g > 50 \text{ GeV}$) as $\epsilon_{\text{fid}} = 45\%$. We assume hadronic-top-tagging [37] and b -tagging efficiencies [43] of $\epsilon_{\text{top}} = \epsilon_b = 50\%$.⁷ From the same PYTHIA sample, we estimate that the soft drop tagging efficiency is $\epsilon_{\text{SD}} = 55\%$, which includes the $p_T^b > 50 \text{ GeV}$, $p_T^g > 25 \text{ GeV}$, and $p_T^g/p_T^b > 0.05$ requirements. The efficiency for the cut $\Theta_b > 1.0$ is $\epsilon_{\Theta_b} = 30\%$, and the S -enriched fraction is $\epsilon_S = 30\%$. This gives an overall signal efficiency of

⁷The corresponding mistag rates from these CMS studies are $\epsilon_{\text{top}}^{\text{mis}} = 5\%$ and $\epsilon_b^{\text{mis}} = 1\%$.

$$\varepsilon_{\text{total}} \approx 0.55\% \quad (16)$$

before placing any restrictions on Θ_S^2 .

For the expected integrated luminosity of $\mathcal{L} = 300 \text{ fb}^{-1}$ to be collected in runs II and III of the LHC by the ATLAS [44] and CMS [45] experiments, we find $\mathcal{N} \approx 1150$ top dead cone candidates. In the crucial phase space region $\Theta_S^2 \in [0.0, 1.0]$, the estimated yield is

$$\mathcal{N}_{\text{on}}^{[0.0, 1.0]} = 85, \quad (17)$$

$$\mathcal{N}_{\text{off}}^{[0.0, 1.0]} = 125, \quad (18)$$

from PYTHIA with and without ME corrections, respectively. The difference between these yields is statistically significant at $\approx 4\sigma$, and the dead cone should be definitively testable with 300 fb^{-1} of LHC data.⁸ A precision differential measurement of the Θ_S^2 spectrum would be possible at higher luminosities, i.e. HL-LHC.

VI. BACKGROUND CONSIDERATIONS

Our analysis thus far has assumed that the dominant background to the dead cone effect is simply b quark FSR from true semileptonic top pair events. That said, secondary backgrounds can arise from single top, W plus jets, and all-hadronic top pairs. These would have to be carefully considered in a full LHC analysis, especially after considering pileup and detector effects, though we estimate here that such backgrounds are negligible.

Single top production actually provides an additional source of signal events if the single top decays leptonically and the recoiling system is mistagged as a boosted hadronic top. If the single top decays hadronically, though, there is a potential source of background events if the recoiling system consists of a (mis)tagged b jet and a W boson. For example, this can occur in t -channel single-top events where the recoiling jet collinearly radiates a leptonic W or in associated production of a single top with a leptonic W boson where there is an additional jet from ISR. Given that the single top cross section is already much smaller than the $t\bar{t}$ cross section, though, such backgrounds yield a subpercent contribution to the total event rate.

For W plus jets, the LO fiducial cross section for $W + b/c + \text{jet}$ with $p_T^j > 500 \text{ GeV}$ and $|\eta^{j,b}| < 2.5$ is estimated to be $\sigma_{Wb,j} \mathcal{B}(W \rightarrow \ell\nu) = 80 \text{ fb}$ with MADGRAPH5_AMC@NLO before any event selection.

⁸Taking a wider interval of $\Theta_S^2 \in [-0.5, 1.5]$, the estimated yield is $\mathcal{N}_{\text{on}}^{[-0.5, 1.5]} = 175$ and $\mathcal{N}_{\text{off}}^{[-0.5, 1.5]} = 235$, which also differs at a significance of $\approx 4\sigma$. Note, however, that the dip in PYTHIA for $\Theta_S^2 \in [-0.5, 0.0]$ is not seen in the other generators.

Note that this cross section incorporates the dominant contribution from dijets, which arises when a boosted dijet system undergoes electroweak FSR, leading to the W plus jets final state already considered. Requiring the light jet to pass a top tag reduces the contribution of this background to the subpercent level.

All-hadronic top pairs are a potential background if the b quark decays semileptonically and one of the W decay products fakes the top radiation. This background can be estimated from simulation, and with the cuts of $p_T^{b,\ell} > 50 \text{ GeV}$ and $p_T^{\text{miss}} > 50 \text{ GeV}$, we estimate that it should contribute at most at the few-percent level. Despite being small, all-hadronic top pairs are likely to be the most important secondary background to consider in a full analysis.

Finally, we note that our $p_T^g > 25 \text{ GeV}$ and $p_T^g/p_T^l > 0.05$ cuts might be too loose given the possibility of pileup jets at high luminosity.⁹ The reason for our cut choice is that the dead cone effect is most robust in the soft gluon limit, up until the point where the interference and bleed-through effect from Eq. (7) becomes relevant. We checked that the qualitative features of our analysis still persist with a soft drop parameter of $z_{\text{cut}} = 0.1$ and harder cuts of $p_T^g > 50 \text{ GeV}$ and $p_T^g/p_T^l > 0.1$, though the statistical significance of the signal with 300 fb^{-1} is degraded down to the 2σ – 3σ level. If a tighter p_T^g cut is needed, then one would likely want to revisit the $p_T^{b,\ell}$ and p_T^{miss} requirements as well, especially if there are alternative methods available to suppress the all-hadronic top background.

VII. CONCLUSIONS

With the excellent performance of the ATLAS and CMS detectors and the high luminosities foreseen at the LHC, together with new analysis techniques based on jet substructure, there is an opportunity to study subtle physics effects involving hadronic final states. For example, jet substructure techniques have previously enabled the study of color flow between the final states in top decay [46–48], an effect that relies on detecting soft gluons from color-connected partons.

In this paper, we have shown how to test the dead cone effect—a universal prediction of gauge theories—in QCD FSR from top quarks. The top quark is rather special in this context, since for bottom and charm quarks, the dead cone effect is obscured both by heavy hadron decays and nonperturbative physics. Focusing on top and antitop pairs with a single-lepton final state, we presented a complete analysis strategy based on the observable Θ_S^2 that can be used to test for the presence of the dead cone effect. Our

⁹Recall, though, that the value of p_T^g is inferred after performing the soft drop procedure, which would certainly help to mitigate the effect of pileup jets.

technique exploits the ability of the soft drop algorithm to reconstruct the angular pattern of the radiated gluon, despite the complications faced by several blurring effects including b quark FSR.

There are four key steps to our procedure. First, we use soft drop to define the candidate b quark and gluon kinematics within a boosted leptonic top. Second, we reconstruct the missing neutrino using the W mass constraint. Third, we select the S -enriched region of phase space where $m_{b\ell\nu} \approx m_t$, such that the gluon is more likely to come from top FSR than from top decay. Finally, we impose a Θ_b angular cut on the candidate b quark to suppress residual contamination from b quark FSR. This leads to a subtle but convincing dead cone suppression in the Θ_S^2 distribution.

In preliminary tests using a fast detector simulation [49], we find that the reconstructed top and gluon kinematics are not dramatically distorted by detector effects, owing partly to the robustness of the soft drop procedure. We therefore look forward to detailed dead cone studies at the LHC, as well as future applications of jet substructure techniques to probe the subtleties of QCD.

ACKNOWLEDGMENTS

We thank Torbjörn Sjöstrand for help validating the dead cone effect in PYTHIA. F.M. would like to thank Scott Willenbrock for inspiring this investigation. This work has been supported by the MIT-Belgium Program of the MIT International Science and Technology Initiatives. The work of F.M. and M.S. has been performed in the framework of the ERC Grant No. 291377 ‘‘LHCTheory’’; it has been supported in part by the European Union as part of the FP7 Marie Curie Initial Training Network MCnetITN (PITN-GA-2012-315877), and in part by the Belgian Federal Science Policy Office through the Interuniversity Attraction Pole P7/37 and by the FNRS. The work of J.T. is supported by the U.S. Department of Energy (DOE) under cooperative research Agreement No. DE-SC-00012567, by the DOE Early Career research program DE-SC-0006389, and by a Sloan Research Fellowship from the Alfred P. Sloan Foundation.

APPENDIX A: EFFECT OF FINAL-STATE INTERFERENCE AND BLEED-THROUGH

As argued in Eq. (7), a cut on the gluon energy fraction is necessary to avoid interference between the top FSR diagram (S) and the top decay diagrams ($B_{1,2}$) as well as to suppress bleed-through of the $B_{1,2}$ diagrams when $m_{b\ell\nu} \approx m_t$. To quantify this, we simulate $e^+e^- \rightarrow tb\ell\nu g$ at tree level with MADGRAPH5_AMC@NLO 2.3.2

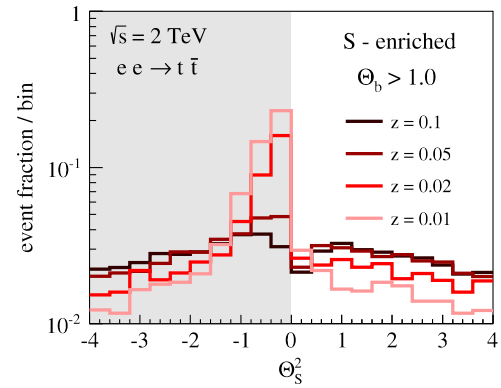


FIG. 9. The Θ_S^2 distribution in $e^+e^- \rightarrow tb\ell\nu g$ events at 2 TeV, for various choices of the minimum gluon energy. The cuts $m_{b\ell\nu} \in [170, 200]$ GeV and $\Theta_b > 1.0$ have been applied in order to reduce direct contamination from radiation in decay. For high enough gluon energies ($z \gtrsim 0.05$), the dead cone pattern is preserved whereas for smaller values ($z \lesssim 0.02$), it is washed out by interference and bleed-through effects.

in order to evaluate the full matrix element including the interference, where the same caveat from footnote 4 applies.

In Fig. 9, we show the Θ_S^2 observable obtained with a set of different cuts on the gluon energy. Here, the final-state kinematics are assumed to be perfectly known, and we apply the same signal selection as the one described in Secs. IV C and IV D. Despite having explicitly suppressed direct contributions from $B_{1,2}$ by requiring $m_{b\ell\nu} \in [170, 200]$ GeV and $\Theta_b > 1.0$, we see that for small gluon energies ($z \lesssim 0.02$), the dead cone is washed out by interference and bleed-through effects, confirming the qualitative arguments given in Sec. III.

APPENDIX B: DISTRIBUTIONS WITHOUT A Θ_b CUT

Previously in Fig. 8, we showed distributions for Θ_S^2 after imposing a cut of $\Theta_b > 1.0$. The motivation for the Θ_b requirement was to increase the statistical significance of the dead cone effect. Here in Fig. 10, we show results corresponding to the same analysis, yet without the Θ_b cut. Comparing the PYTHIA distributions with ME corrections on and off, a statistically significant difference of roughly 3σ after 300 fb^{-1} can be observed. The expected characteristic distribution of the radiation, however, is washed out, leading to a plateau between $0 < \Theta_S^2 < 1$ instead of a suppression towards the origin. We therefore conclude that a Θ_b cut will likely be needed to gain confidence in the dead cone effect.

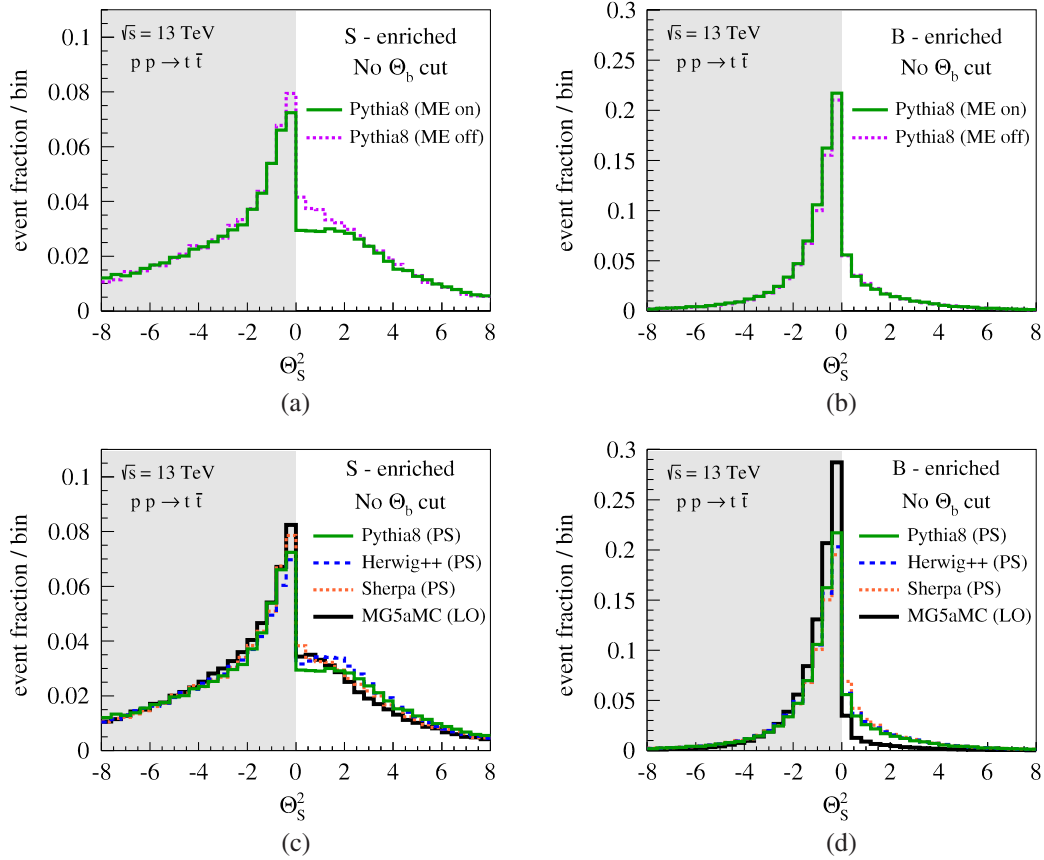


FIG. 10. The same as Figs. 8(a), 8(b), 8(c), and 8(d), but without a cut on Θ_b .

APPENDIX C: IDEALIZED DISTRIBUTIONS WITH REALISTIC CUTS

As mentioned in Sec. IV D, ISR and UE are sources of jet contamination that partially fill the dead cone in pp collisions. To understand the effect of this contamination on our analysis, we return to e^+e^- collisions and use them as a template where ISR and UE effects are absent. We then perform the exact same LHC-targeted analysis from Sec. IV, with the

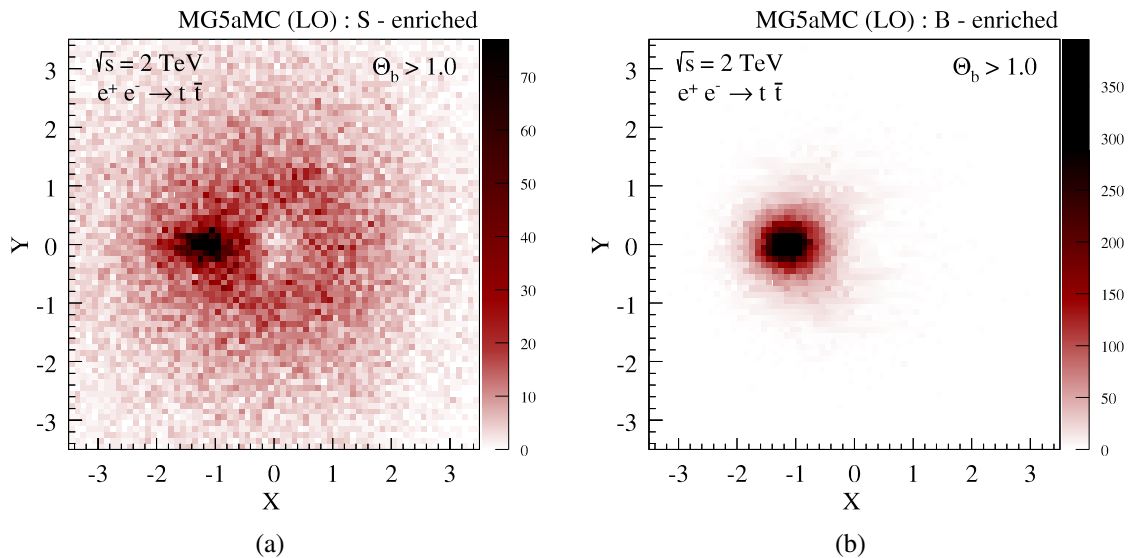


FIG. 11. The same as Figs. 7(a) and 7(b), but applying our analysis strategy on $e^+e^- \rightarrow t\bar{t}$ events at $\sqrt{s} = 2$ TeV.

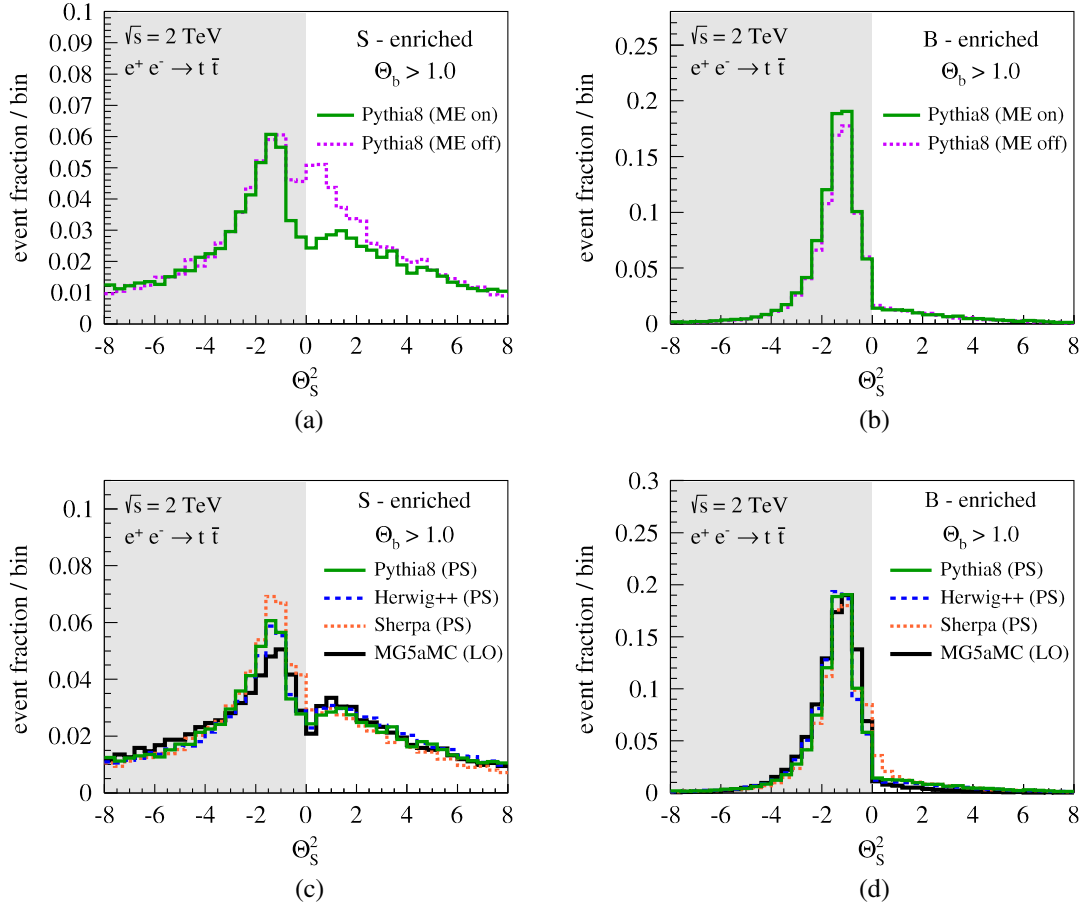


FIG. 12. The same as Figs. 8(a), 8(b), 8(c), and 8(d), but applying our analysis strategy on $e^+e^- \rightarrow t\bar{t}$ events at $\sqrt{s} = 2 \text{ TeV}$.

corresponding e^+e^- results shown in Figs. 11 and 12. The overall qualitative features are the same as in the pp case. As expected, though, the differences between the ME-on and ME-off PYTHIA distributions are more noticeable in the e^+e^- case, and the dip towards $\Theta_S^2 = 0$ is more pronounced.

-
- [1] Y.L. Dokshitzer, V.A. Khoze, and S.I. Troian, Particle spectra in light and heavy quark jets, *J. Phys. G* **17**, 1481 (1991).
- [2] Y.L. Dokshitzer, V.A. Khoze, and S.I. Troian, On specific QCD properties of heavy quark fragmentation (“dead cone”), *J. Phys. G* **17**, 1602 (1991).
- [3] R. Keith Ellis, W.J. Stirling, and B.R. Webber, QCD and collider physics, Cambridge Monogr. Part. Phys., Nucl. Phys. Cosmol. **8**, 1 (1996).
- [4] B.A. Schumm, Y.L. Dokshitzer, V.A. Khoze, and D.S. Koetke, MLLA and the Average Charged Multiplicity of Events Containing Heavy Quarks in e^+e^- Annihilation, *Phys. Rev. Lett.* **69**, 3025 (1992).
- [5] Y.L. Dokshitzer, V.A. Khoze, and S.I. Troian, Specific features of heavy quark production. LPHD approach to heavy particle spectra, *Phys. Rev. D* **53**, 89 (1996).
- [6] Y.L. Dokshitzer, F. Fabbri, V.A. Khoze, and W. Ochs, Multiplicity difference between heavy and light quark jets revisited, *Eur. Phys. J. C* **45**, 387 (2006).
- [7] A. Perieanu, Ph.D. thesis, Hamburg University, 2006.
- [8] J. Abdallah *et al.* (DELPHI Collaboration), Study of b-quark mass effects in multijet topologies with the DELPHI detector at LEP, *Eur. Phys. J. C* **55**, 525 (2008).
- [9] G. Marchesini and B.R. Webber, Simulation of QCD coherence in heavy quark production and decay, *Nucl. Phys.* **B330**, 261 (1990).
- [10] K. Okabe *et al.* (VENUS Collaboration), Measurement of the charged multiplicity of bottom and light quark events in e^+e^- annihilation at $s^{**}(1/2) = 58\text{-GeV}$, *Phys. Lett. B* **423**, 407 (1998).
- [11] R. Perez Ramos, V. Mathieu, and M.-A. Sanchis-Lozano, Heavy quark flavour dependence of multiparticle

- production in QCD jets, *J. High Energy Phys.* **08** (2010) 047.
- [12] R. J. Barlow *et al.*, Report of the heavy flavors working group, *J. Phys. G* **17**, 1605 (1991).
- [13] M. Battaglia, R. Orava, and L. Salmi, CERN Technical Reports No. DELPHI-2004-037-CONF-712 and No. CERN-DELPHI-2004-037-CONF-712, 2004.
- [14] S. V. Chekanov, Soft gluon angular screening in heavy quark fragmentation, *Phys. Lett. B* **484**, 51 (2000).
- [15] D. E. Soper and M. Spannowsky, Finding top quarks with shower deconstruction, *Phys. Rev. D* **87**, 054012 (2013).
- [16] A. Abdesselam *et al.*, Boosted objects: A probe of beyond the standard model physics, *Eur. Phys. J. C* **71**, 1661 (2011).
- [17] A. Altheimer *et al.*, Jet substructure at the Tevatron and LHC: New results, new tools, new benchmarks, *J. Phys. G* **39**, 063001 (2012).
- [18] A. Altheimer *et al.*, Boosted objects and jet substructure at the LHC, *Eur. Phys. J. C* **74**, 2792 (2014).
- [19] D. Adams *et al.*, Towards an understanding of the correlations in jet substructure, *Eur. Phys. J. C* **75**, 409 (2015).
- [20] A. J. Larkoski, S. Marzani, G. Soyez, and J. Thaler, Soft drop, *J. High Energy Phys.* **05** (2014) 146.
- [21] J. M. Butterworth, A. R. Davison, M. Rubin, and G. P. Salam, Jet Substructure as a New Higgs Search Channel at the LHC, *Phys. Rev. Lett.* **100**, 242001 (2008).
- [22] D. Krohn, J. Thaler, and L.-T. Wang, Jet trimming, *J. High Energy Phys.* **02** (2010) 084.
- [23] S. D. Ellis, C. K. Vermilion, and J. R. Walsh, Techniques for improved heavy particle searches with jet substructure, *Phys. Rev. D* **80**, 051501 (2009).
- [24] S. D. Ellis, C. K. Vermilion, and J. R. Walsh, Recombination algorithms and jet substructure: Pruning as a tool for heavy particle searches, *Phys. Rev. D* **81**, 094023 (2010).
- [25] M. Dasgupta, A. Fregoso, S. Marzani, and G. P. Salam, Towards an understanding of jet substructure, *J. High Energy Phys.* **09** (2013) 029.
- [26] A. J. Larkoski, S. Marzani, and J. Thaler, Sudakov safety in perturbative QCD, *Phys. Rev. D* **91**, 111501 (2015).
- [27] G. Altarelli and G. Parisi, Asymptotic freedom in parton language, *Nucl. Phys.* **B126**, 298 (1977).
- [28] J. Alwall, R. Frederix, S. Frixione, V. Hirschi, F. Maltoni, O. Mattelaer, H.-S. Shao, T. Stelzer, P. Torrielli, and M. Zaro, The automated computation of tree-level and next-to-leading order differential cross sections, and their matching to parton shower simulations, *J. High Energy Phys.* **07** (2014) 079.
- [29] T. Sjostrand, S. Mrenna, and P. Z. Skands, PYTHIA 6.4 physics and manual, *J. High Energy Phys.* **05** (2006) 026.
- [30] T. Sjostrand, S. Mrenna, and P. Z. Skands, A brief introduction to PYTHIA 8.1, *Comput. Phys. Commun.* **178**, 852 (2008).
- [31] E. Norrbin and T. Sjostrand, QCD radiation off heavy particles, *Nucl. Phys.* **B603**, 297 (2001).
- [32] M. Bahr *et al.*, Herwig ++ physics and manual, *Eur. Phys. J. C* **58**, 639 (2008).
- [33] T. Gleisberg, S. Hoeche, F. Krauss, M. Schonherr, S. Schumann, F. Siegert, and J. Winter, Event generation with SHERPA 1.1, *J. High Energy Phys.* **02** (2009) 007.
- [34] Y. L. Dokshitzer, V. A. Khoze, L. H. Orr, and W. J. Stirling, Properties of soft radiation near $t\bar{t}$ and W^-W^- threshold, *Nucl. Phys.* **B403**, 65 (1993).
- [35] L. H. Orr, Y. L. Dokshitzer, V. A. Khoze, and W. J. Stirling, Gluon radiation and top width effects, [arXiv:hep-ph/9307338](https://arxiv.org/abs/hep-ph/9307338).
- [36] V. A. Khoze, J. Ohnemus, and W. James Stirling, Soft gluon radiation in hadronic t anti-t production, *Phys. Rev. D* **49**, 1237 (1994).
- [37] S. Chatrchyan *et al.* (CMS Collaboration), Technical Report No. CMS-PAS-JME-13-007, 2014.
- [38] M. Cacciari, G. P. Salam, and G. Soyez, The anti-k(t) jet clustering algorithm, *J. High Energy Phys.* **04** (2008) 063.
- [39] M. Cacciari, G. P. Salam, and G. Soyez, FastJet user manual, *Eur. Phys. J. C* **72**, 1896 (2012).
- [40] Y. L. Dokshitzer, G. D. Leder, S. Moretti, and B. R. Webber, Better jet clustering algorithms, *J. High Energy Phys.* **08** (1997) 001.
- [41] A. J. Larkoski and J. Thaler, Aspects of jets at 100 TeV, *Phys. Rev. D* **90**, 034010 (2014).
- [42] M. Czakon, P. Fiedler, and A. Mitov, Total Top-Quark Pair-Production Cross Section at Hadron Colliders Through $O(\frac{\alpha_s^3}{s})$, *Phys. Rev. Lett.* **110**, 252004 (2013).
- [43] S. Chatrchyan *et al.* (CMS Collaboration), Identification of b-quark jets with the CMS experiment, *J. Instrum.* **8**, P04013 (2013).
- [44] G. Aad *et al.* (ATLAS Collaboration), Expected performance of the ATLAS experiment—Detector, trigger and physics, [arXiv:0901.0512](https://arxiv.org/abs/0901.0512).
- [45] G. L. Bayatian *et al.* (CMS Collaboration), Technical Reports No. CERN-LHCC-2006-001 and No. CMS-TDR-008-1, 2006.
- [46] J. Gallicchio and M. D. Schwartz, Seeing in Color: Jet Superstructure, *Phys. Rev. Lett.* **105**, 022001 (2010).
- [47] V. M. Abazov *et al.* (D0 Collaboration), Measurement of color flow in $t\bar{t}$ events from $p\bar{p}$ collisions at $\sqrt{s} = 1.96$ TeV, *Phys. Rev. D* **83**, 092002 (2011).
- [48] G. Aad *et al.* (ATLAS Collaboration), Measurement of colour flow with the jet pull angle in $t\bar{t}$ events using the ATLAS detector at $\sqrt{s} = 8$ TeV, *Phys. Lett. B* **750**, 475 (2015).
- [49] J. de Favereau, C. Delaere, P. Demin, A. Giammanco, V. Lemaître, A. Mertens, and M. Selvaggi (DELPHES 3 Collaboration), DELPHES 3, A modular framework for fast simulation of a generic collider experiment, *J. High Energy Phys.* **02** (2014) 057.